INTERNATIONAL JOURNAL OF CLIMATOLOGY
Int. J. Climatol. (2017)
Published online in Wiley Online Library
(wileyonlinelibrary.com) DOI: 10.1002/joc.5051

RMetS
Royal Meteorological Society

Convection regimes and tropical-midlatitude interactions over the Intra-American Seas from May to November

N. Vigaud* and A.W. Robertson

International Research Institute for Climate and Society, IRI, Earth Institute at Columbia University, New York, NY, USA

ABSTRACT: A cluster analysis is applied to National Oceanic and Atmospheric Administration daily outgoing longwave radiation anomaly fields over the Intra-American Seas, for the May to November rainy season 1980–2009. Seven recurrent convection regimes are identified, each with distinct impacts on local rainfall. Three suppressed-convection regimes prevailing throughout the season and in particular during the Mid-Summer Drought are related to transient anticyclonic circulation anomalies and broad drying over the region. The remaining regimes are all related to enhanced convection and cyclonic circulation anomalies over the Caribbean. For one wet regime, the cyclonic anomaly is located over Central America, which increases moisture advection from the eastern Pacific and in turn rainfall over Central and South America to the disadvantage of northern regions of the Caribbean. The three other regimes are associated with a weaker Caribbean Low Level Jet along its southern branch stretching along the South American coast, while its northern branch is strengthened, exposing the Caribbean to more moisture advection from the northeast trade winds, enhancing convection and rainfall locally. These three wet regimes are related to northwestward-propagating convective cells that can be traced in a composite sense to the southward incursion of baroclinic waves from the midlatitudes, and anticyclonic wave breaking. In addition, their frequencies are found to be higher during phases 1 and 2 of the Madden-Julian Oscillation, suggesting a connection with easterly waves emanating from African convection. Relationships are shown between these three northwestward-propagating wet regimes and historical floods in the Caribbean illustrating the potential value of the convective regime approach for ultimately improving regional predictions and disaster early warning on sub-seasonal scales.

KEY WORDS sub-seasonal convection variability; weather typing; tropical-midlatitudes interactions; IAS rainfall; Caribbean floods

Received 8 June 2016; Revised 1 February 2017; Accepted 7 February 2017

1. Introduction

Commonly defined as the region extending from the eastern tropical Pacific to the western tropical North Atlantic, the Intra-American Seas (IAS) which includes both the Gulf of Mexico and the Caribbean Sea, is a unique region of spatiotemporal scale interactions on time-scales ranging from diurnal to inter-annual and longer, and on spatial scales from a few to thousands of kilometres. Regional climate is known to be influenced locally by sea breezes and low-level winds such as the Intra-America or Caribbean Low Level Jet (CLLJ), tropical cyclones (TCs) and easterly wave activity, all modulated by larger scale processes such as the Madden-Julian Oscillation (MJO), the latitudinal migration of the Intertropical Convergence Zone (ITCZ), the El Niño Southern Oscillation (ENSO) and the Atlantic Multi-decadal Oscillation (AMO) amongst others (Hidalgo *et al.*, 2015; Serra *et al.*, 2016). It is thus an excellent test case for exploring intra-seasonal convection variability, its relationships to regional rainfall and the atmospheric circulation in the Tropics, as well as at higher latitudes, and modulations by large-scale climate signals. Based on the hypothesis that large-scale atmospheric patterns tend to repeatedly establish over fixed locations (Vautard *et al.*, 1990; Moron *et al.*, 2008), and that their persistence translates into significant regional climate anomalies (Michelangeli *et al.*, 1995; Ghil and Robertson, 2002), weather types can be seen as intrinsic regimes of weather that can be modulated at different time-scales, and are used in the following to identify recurrent convection regimes during the extended hurricanes season (May–November), when local societies are most vulnerable.

On planetary scales, topography together with continental and oceanic heating contrast force the North American and South American Monsoon Systems (NAMS and SAMS), which have both been related to IAS summer precipitation (Figueroa and Nobre, 1990; Mock, 1996; Higgins *et al.*, 1997). An important regional feature of the monsoonal circulation that develops during both boreal summer and winter is the CLLJ, which is closely related to the strength and position of the North Atlantic Subtropical High (NASH). The CLLJ is modulated by the atmospheric response to sea-land temperature contrast caused by the distribution of American land masses (Amador, 1998, 2008). The CLLJ is located at about [12.5°–17.5°N;

* Correspondence to: N. Vigaud, International Research Institute for Climate and Society (IRI), Earth Institute at Columbia University, 61 Rte 9W, Palisades, NY 10964, USA. E-mail: nicolas.vigaud@gmail.com

70°–80°W] where it exhibits a peak in July before it weakens in September to reach another maximum in January. Windspeeds within the CLLJ core vary in phase with the North Atlantic Oscillation (NAO) in winter through modulations in strength of the NASH, while during summer a strong (weak) CLLJ is related to a weak (strong) summer monsoon (Wang, 2007). In July, the westward extension of the NASH leads to maximum wind speeds above 10 m s^{-1} at the CLLJ core (Wang and Lee, 2007), which by then extends up to 700 hPa (Amador, 2008; Whyte *et al.*, 2008). Noteworthy, the summer component of the CLLJ splits into two branches over the Caribbean, one veering northward, eventually connecting with the Great Plains Low Level Jet (GPLLJ), and another crossing Central America towards the Pacific (Amador, 2008; Cook and Vizy, 2010).

Descent prevails over the Caribbean in summer and it is the passage of transient systems that produce precipitation over the region. These are associated with easterly wave activity in summer and fall (Serra *et al.*, 2010) which coincides with the TC season from July to October (Frank and Roundy, 2006). Some of these westward-propagating tropical disturbances originating over Africa grow into hurricanes (Thorncroft *et al.*, 2003; Xie and Carton, 2004), while TC activity peaks when the vertical wind shear is weakest in July–August (Aiyyer and Thorncroft, 1997). The climatological rainfall season spans roughly from May to November (Enfield and Alfaro, 1999; Giannini *et al.*, 2000) and is generally divided into the early (May–July) and late (August–November) rainy seasons, with a rainfall minimum in July–August referred to as the Mid-Summer Drought (MSD) associated with the westward enhancement of the subtropical high (Hastenrath, 1984; Enfield and Alfaro, 1999; Magana *et al.*, 1999; Giannini *et al.*, 2000, 2001; Taylor *et al.*, 2002; Angeles *et al.*, 2010).

At inter-annual time-scales, IAS climate is influenced by ENSO, which is negatively correlated to Caribbean summer rainfall. The warm (cold) ENSO phases are associated during year 0, with a stronger (weaker) CLLJ and colder (warmer) SSTs in the tropical North Atlantic (Hastenrath and Lamb, 1977; Ropolewski and Halpert, 1987; Enfield and Alfaro, 1999; Magana *et al.*, 1999; Giannini *et al.*, 2000; Chen and Taylor, 2002; Taylor *et al.*, 2002; Wang and Lee, 2007). ENSO influences Caribbean climate directly via a zonal seesaw in sea level pressures (SLPs) between the tropical Pacific and Atlantic basins that modulates surface heat fluxes in the tropical Atlantic and lead to local SST anomalies there (Enfield and Mayer, 1997; Chang *et al.*, 2003), as well as via an anomalous meridional overturning circulation during summer which connects the vertical motions over both basins (Wang *et al.*, 2010). In addition, ENSO exerts indirect influences through its lagged effect on tropical Atlantic SSTs via a wave train reminiscent of the Pacific North American (PNA) pattern (Enfield and Mayer, 1997; Giannini *et al.*, 2000; Chen and Taylor, 2002; Taylor *et al.*, 2002). The tropical Atlantic surface conditioning can sustain or weaken ENSO-induced rainfall variability (Wu and Kirtman, 2010), and peak Caribbean rainfall are generally associated with highest SSTs in the tropical Atlantic warm pool (Taylor *et al.*, 2002; Wang *et al.*, 2006; Wang and Lee, 2007) in conjunction with SLP anomalies modulating the NASH (Enfield and Alfaro, 1999; Giannini *et al.*, 2000) and local SSTs/SLPs gradients (Enfield and Alfaro, 1999; Giannini *et al.*, 2000; Taylor *et al.*, 2002, 2011). Warmer conditions in the tropical Atlantic during the early rainy season tend to sustain tropical easterly waves, which originate from Africa, across the Atlantic basin, leading to more convection and rainfall (Taylor *et al.*, 2002). In addition, the number of Atlantic hurricanes varies with the size of the warm pool due to increased local heat content, reduced vertical wind shear and increased moist static instability (Wang and Lee, 2007). Overall, cool (warm) SST anomalies in the tropical Atlantic and a warmer (cooler) tropical Pacific modify the zonal SST gradient reducing (increasing) moisture convergence and precipitation (Taylor *et al.*, 2011).

At intra-seasonal time-scales, easterly waves are a prominent feature of the Atlantic ITCZ (Serra *et al.*, 2010). While these waves generally weaken as they traverse the relatively cool central Atlantic, Shapiro (1996) found evidence that African Easterly Waves (AEWs) with periodicities below 10 days, do propagate across the basin where they are characterized by dissipative Rossby wave packets (Molinari *et al.*, 1996). These waves have often been found to be trackable into the Caribbean (Carlson, 1969; Thorncroft and Hodges, 2001; Kerns *et al.*, 2008; Serra *et al.*, 2010). Recent studies (Leroux and Hall, 2010; Ventrice *et al.*, 2011; Yu *et al.*, 2011) have emphasized substantial influences of the MJO (30–60 days cycle) on AEW over Africa during Northern Hemisphere summer. During phases 1 and 2 (5 and 6), when MJO convection is located in Africa and the western Indian Ocean (in the western Pacific), cyclogenesis is increased (decreased) in the tropical Atlantic in association with more (less) frequent and strong AEW but also modulations of vertical wind shear, moisture and low-level cyclonic relative vorticity over the basin (Ventrice *et al.*, 2011). It is thus during phases 1 and 2 (5 and 6) that extreme rainfall events over the Caribbean islands are generally most pronounced (substantially reduced) through weakened (strengthened) easterly trades and CLLJ with low-level divergence anomalies at the entrance/exit of the jet leading precipitation anomalies, especially from September to November (Martin and Schumacher, 2011).

While regional climate variability was long recognized to be related to wave perturbations in the easterly trades, Riehl (1945, 1948) was amongst the first to note the substantial role of extra-tropical troughs in the development of heavy rainfall events in the basin. This was confirmed two decades later by Yanai (1968) who emphasized the potential importance of their interactions with easterly waves, an aspect that still need to be further studied. From the perspective of the multiplicity of impacts on IAS rainfall across various time-scales, the goal of this study is to diagnose sub-seasonal convection variability over the IAS, together with its intra-seasonal to inter-annual modulations, by clustering daily OLR observations from May to November. The associated atmospheric circulation anomalies are analysed through compositing of reanalysis data with a particular focus on potential interactions between the Tropics and midlatitudes, alongside their relationships to regional rainfall and large-scale surface temperatures in the neighbouring oceanic basins. The article is outlined as follows. The data and method are presented in Section 2. Results from the cluster analysis are then discussed in Section 3. Relationships to rainfall and associated atmospheric circulation anomalies are presented for specific wet convection regimes in Section 4. Summary and conclusions are gathered in Section 5.

2. Data and methods

2.1. Datasets

Tropical convection is examined from May to November using daily OLR produced by the National Oceanic and Atmospheric Administration (NOAA) and available on a $2.5° \times 2.5°$ regular grid from 1979 to present (Liebmann and Smith, 1996). While the coarse spatial resolution of OLR does not allow us to capture individual meso-scale convective systems (thunderstorms, cloud clusters), it is their synoptic-scale organization that is of interest in this article.

This study makes use of gridded daily rainfall estimates from the Climate Hazards group InfraRed Precipitation with Station dataset (CHIRPS) developed at the University of California at Santa Barbara (UCSB) Climate Hazards Group (CHG) in collaboration with the US Geological Survey (USGS) Earth Resources Observation and Science (EROS) center (Funk *et al.*, 2014). These data are at 0.05° latitude–longitude resolution. While CHIRPS data also includes satellite information, it is one of the few available datasets covering the whole region at daily time-scales that has data back to the 1980s, and have been validated in recent studies including over the IAS region (Funk *et al.*, 2015). NOAA OLR comes from polar orbiting satellites, while CHIRPS rainfall estimates contain remote sensing information from geostationary satellites, and thus may be considered as independent (Vigaud *et al.*, 2017). *In situ* rainfall estimates from the gauge based unified precipitation dataset developed by NOAA and the National Centers for Environmental Prediction (NCEP) Climate Prediction Center (also referred to as NOAA Unified rainfall), offering gridded daily values from 1980 to near-present at a $0.5° \times 0.5°$ spatial resolution, were also used to further confirm the relationships emphasized with CHIRPS rainfall (NOAA Unified rainfall leads to similar results, not shown). Since both of these precipitation datasets cover land areas only, TRMM 3B42 v7 daily satellite estimates (Huffman *et al.*, 2010) are also considered for the 1998–2009 period, to relate anomalies over land with anomalous patterns prevailing over the IAS. Moreover, historical flooding events, compiled in the Caribbean Disaster Impacts and Preparedness database at the Caribbean Institute for Meteorology and Hydrology (CIMH) in Barbados, are used to identify potential relationships with past episodes at island-scale.

Daily atmospheric fields from the NCEP-DOE II reanalysis (NCEP2 in the following), produced jointly by NCEP and the Department Of Energy (DOE) in the United States, at $2.5° \times 2.5°$ horizontal resolution (Kanamitsu *et al.*, 2002), are used to investigate relevant atmospheric circulation features affecting the region. Amongst these, we chose to focus mainly on prevailing low-level and surface conditions, AEW activity and upper-level westerly waves by considering, winds, geopotentials and omega vertical velocities. The relationships between each convection regime and SSTs in the different oceanic basins are assessed using the NOAA Optimum Interpolation SST version 2 (OISST) dataset consisting of daily values at a quarter of a degree (Reynolds *et al.*, 2007), which where aggregated for May–November seasons from 1982 to 2009.

2.2. Dynamical clustering approach

In this article, sub-seasonal convection activity is examined using a methodology which has been applied successfully in previous studies for the Caribbean and other regions of the globe (Fauchereau *et al.*, 2009; Vigaud *et al.*, 2012, 2017; Moron *et al.*, 2015; Saenz and Duran-Quesada, 2015). Daily OLR anomalies are obtained by subtracting the mean annual cycle on a daily basis, which are input into an objective classification through *k*-means clustering (Michelangeli *et al.*, 1995; Cheng and Wallace, 2003) over the domain [7.5°–30°N; 57.5°–96°W] centred over the Caribbean Sea and Gulf of Mexico. To reduce the dimensionality of the problem and to ensure linear independence between input variables, an EOF analysis is first performed on the data correlation matrix and the first 11 PCs, explaining 62.5% of the variance, are retained. The Euclidean distance is then used to measure similarities between daily OLR patterns and a given regime. The robustness of regime partitions is then measured by a classifiability index (Cheng and Wallace, 2003) and compared to confidence limits from a red-noise test (applied to Markov-generated red-noise data) following previous studies (Michelangeli *et al.*, 1995; Moron and Plaut, 2003; Fauchereau *et al.*, 2009; Vigaud *et al.*, 2012, 2017).

Results from composites related to each daily OLR regime are tested for statistical significance using a parametric test, the two-tailed Student's *t*-test, comparing the means of the total fields from all days belonging to a regime *versus* the May–November mean over the 30-year study period.

3. Daily regimes of anomalous convection over the IAS

To identify daily convection regimes during the May to November season over the 1980–2009 period, *k*-means clustering is applied on May to November NOAA daily OLR anomalies over [0°–30°N; 57.5°–96°W] (Figure 2(a)) following the methodology described in Section 2.2. The corresponding *k*-means classifiability index (Figure 1)

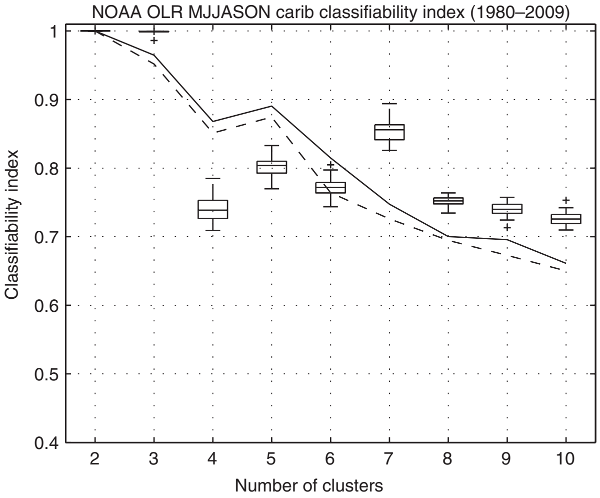

Figure 1. Classifiability index as a function of the number of regimes k (boxes). The levels of significance at 95/90% (solid/dashed) are computed according to a first-order Markov process.

exhibits a significant peak for $k = 7$ and larger values. However, the 7-cluster partition is the most compact and highly significant solution, which has thus been selected for the subsequent analysis. Figure 2 displays each regime's daily OLR anomalies, with respect to the mean seasonal cycle, projected over a broader IAS region by compositing over all days assigned to each cluster.

The first regime is characterized by large-scale positive OLR anomalies indicating reduced convection over the IAS. During regime 2, positive anomalies also dominate the region with highest loadings centred at about 16°N and 60°W as well as 24°N and 80°W. These indicate reduced convection over most of the IAS with the exception of the southern parts of the region near the Panama Isthmus, where negative OLR anomalies and thus enhanced convection prevail. Regimes 3, 4, 5 and 6 display alternating negative and positive OLR anomalies orientated in a SE-NW band. With the exception of regime 3 for which positive OLR anomalies prevail over the IAS, the strongest anomalies are negative and surrounded by positive anomalies upstream/downstream (i.e. to the NW/SE): such patterns could be characteristic of convective cells entering the Caribbean from the southeast and travelling northwestwards across the basin. The May–November period corresponds to the hurricane season and interestingly, these patterns are consistent with the trajectories of some TCs that have developed over the Caribbean, particularly the fourth cluster presented in Kossin *et al.* (2010). Finally, regime 7 is characterized by large-scale negative OLR anomalies prevailing between 45° and 110°W from the Equator to about 25°N. Anomalies of opposite sign and weaker in magnitude are found east of 75°W north of 20°N, nevertheless maximum positive loadings are organized in a pattern typical of the ITCZ when at its northernmost location in summer and indicate enhanced convection processes along the northern coast of South America, including Central America and the eastern Caribbean.

Transitions between the seven OLR regimes are illustrated in Table 1 obtained by counting for each day and each regime, the regime occurring the following day. Highest counts are found along the diagonal indicative of the persistence of each regime at daily time-scale. Significant transition probabilities compared to chance are found between the different regimes supporting the idea that some of these classes tend to be related to others with preferential sequences. From Table 1, regime 1 is preferentially followed by regime 2, both associated with reduced convection processes over the region. On the other hand, regimes 3 and 7 tend to precede regime 4. Regime 4 is often followed by regime 5, which is preferentially followed by regime 6. Hence, regimes 3 and 7 appear to be at the beginning of a preferential sequence from regime 4 to regimes 5 and 6. These confirm the interpretation of Figure 2 relating the latter regimes to convective cells propagating across the basin in a northwestward direction. Five major hurricanes that brought devastating damage to the Caribbean – Opal in 1995, Ivan in 2004, Dennis and Wilma in 2005, Ike in 2008 – all correspond to the sequence of regimes 4–5 and 6 (not shown) further illustrating linkages to TCs activity in the tropical Atlantic-Caribbean sector.

The number of occurrences of each regime is broken down by calendar month in Figure 3, recalling that the OLR anomalies are defined with respect to the mean seasonal cycle on a daily basis. Regimes 1 and 2 predominate over most of the season consistent with the highest scores shown in Table 1, highlighting the fact that precipitation over the region is mainly due to the passage of intermittent transient systems such as those represented by regimes 4–6. July–August exhibits highest frequency of regime 2 when it outnumbers regime 1 from then until the end of the season, while the beginning of the season (May–Jun) is characterized by the prevalence of regime 1. Thus, the proportion of regime 1 decreases from May to November, while regime 2 becomes more frequent as the season advances with a marked increase from June to August. It is noteworthy that regime 1 occurrences also display a local maximum in August. Hence, almost half of the days are accounted for by regimes 1 and 2 during the MSD which is consistent with low convection and rainfall during this period. The May–November season is however characterized by occurrences of other regimes most of which are related to the transit of convective cells: regime 4 shows the lowest number of occurrences from May to November, it is followed by regimes 5, 7, 6 and 3. Except regime 3 which is characterized by reduced convection over the IAS and a weak maximum of occurrences in July–August during the MSD, these regimes all exhibit a decrease of their proportion of occurrences in July–August. Their frequencies increase after the MSD with the exception of regime 7 showing a local minimum in October. Regime 6 however is characterized by a quite constant number of occurrences throughout the whole May–November period. Regimes 7 and 5 appear to be almost anti-correlated, with a decrease (increase) of regime 7 (5) prevalence from May to November. Regime 5 is most frequent from August onwards while maximum occurrences of regime 7 are found in July

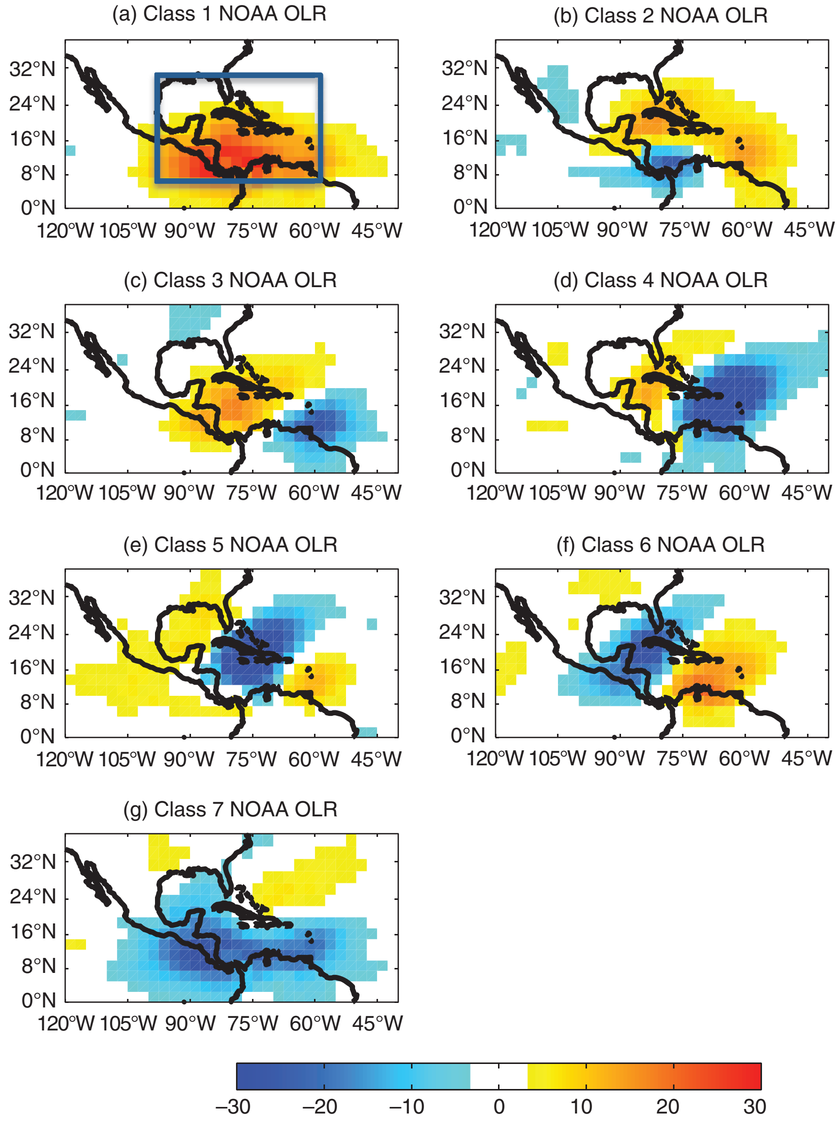

Figure 2. Mean 1980–2009 May–November NOAA daily OLR (in W m^{-2}) for the seven convection regimes identified. Only the grid-points for which anomalies are significant at 95% confidence level of Student's *t*-test are displayed. The blue box in panel (a) denotes the domain used for clustering.

Table 1. Contingency tables between the seven daily OLR classes from NOAA. In parentheses are indicated the respective transition probabilities (in %) obtained by dividing separate class counts by the sum of the columns for each row.

From\To	Class 1	Class 2	Class 3	Class 4	Class 5	Class 6	Class 7
Class 1	631*(53.75*)	240*(20.44*)	169 (14.40)	14 (1.19)	24 (2.04)	84 (7.16)	12 (1.02)
Class 2	172 (14.73)	496*(42.47*)	144 (12.33)	35 (2.99)	75 (6.42)	130 (11.13)	116 (9.93)
Class 3	117 (12.20)	161 (16.79)	401*(41.81*)	110*(11.47*)	25 (2.61)	54 (5.63)	91 (9.49)
Class 4	48 (7.87)	41 (6.72)	47 (7.71)	298*(48.85*)	101*(16.56*)	18 (2.95)	57 (9.34)
Class 5	65 (8.92)	38 (5.22)	35 (4.80)	35 (4.80)	367*(50.34*)	129*(17.69*)	60 (8.23)
Class 6	133 (14.04)	137 (14.47)	86 (9.08)	10 (1.06)	57 (6.02)	433*(45.72*)	91 (9.61)
Class 7	8 (1.00)	57 (7.10)	74 (9.21)	107*(13.32*)	83 (10.34)	100 (12.45)	374*(46.58*)

*The scores indicated are significant at 99.9% level of χ^2 test.

consistent with the ITCZ northernmost footprint evidenced over northern South America in Figure 2(g). Regime 4 exhibits a minimum number of occurrences in August but highest frequency in October concomitant with maximum number of occurrences of regimes 5 and 6 which also prevail in November.

To summarize, anomalous convection regimes over the Caribbean consist of three suppressed convection regimes (1, 2 and 3) prevailing throughout the season and in particular during the MSD, and four enhanced convection regimes. One of these (regime 7) is most frequent in July and related to anomalous convection over Central

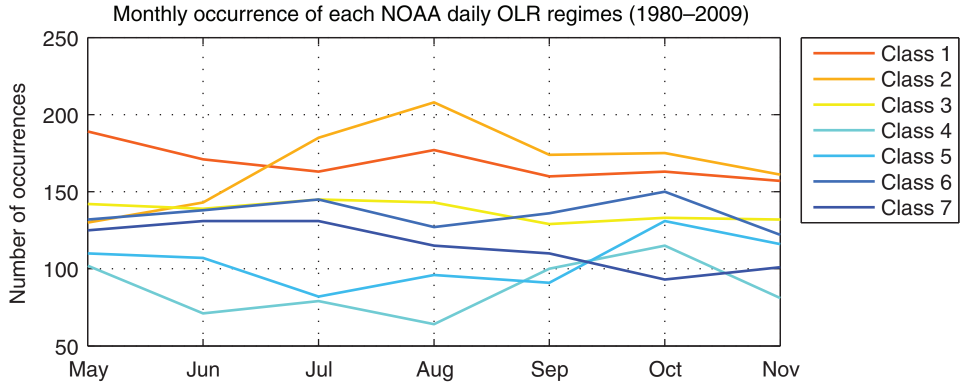

Figure 3. Average counts of the occurrences of each convective regime by calendar month.

and South America, while the remaining three (4, 5 and 6) are all associated with westward propagating convective anomalies developing preferentially from August onwards.

4. Propagating convective cells

Rainfall anomaly composites based on CHIRPS and TRMM daily estimates are plotted in Figure 4 for the days assigned to each cluster. There is a near one-to-one local correspondence between the polarity of the convection anomalies and rainfall anomaly estimates for all seven regimes over both land and ocean, consistent with the convective nature of Caribbean rainfall. Regimes 1, 2 and 3 are all related to negative rainfall anomalies over the IAS region (Figures 4(a)–(c) and (h)–(j)) and will not be discussed further. Regime 7 is associated with anomalously wet conditions over Central and northern South America (Figures 4(g) and (n)), while regimes 4, 5 and 6 show anomalous wet conditions transiting from the southeast to the northwest of the Caribbean. Highest positive rainfall anomalies are located over northern South America, the Lesser Antilles and Hispanola for regime 4 (Figures 4(d) and (k)), migrating to southern Central America, the Greater Antilles and the Bahamas during regime 5 (Figures 4(e) and (l)), while regime 6 is associated with enhanced rainfall extending across Central America with significant wettening pertaining over western Cuba and the Bahamas (Figures 4(f) and (m)). In the following, we will focus on westward propagating convection anomalies represented by regimes 4, 5 and 6 examining in particular their relationships with easterly waves and upper-level midlatitude troughs.

4.1. Regional rainfall and atmospheric circulation anomalies

Anomaly composites of reanalysis data are shown in Figures 5–9, again defining anomalies with respect to the mean seasonal cycle on a daily basis. Concomitant with regimes 4–6 westward progression of anomalous convection and wet conditions across the basin, a cell of negative geopotential anomalies is seen to move from about 65°W for regime 4 to 90°W between 18° and 24°N for regimes 5 and 6 (Figure 5, left panels, shading). This low pressure cell is associated with a northwestward propagating cyclonic circulation anomaly increasing in intensity from regime 4 to 5, and decreasing from regime 5 to 6. Significant negative wind speed anomalies in regime 4 are centred at 12°N and 75°W together with positive anomalies maximum at 22°N and 68°W (Figure 5(a), contours). These wind speed anomalies imply a weakening of the CLLJ along its southern branch and enhanced trades along its northern branch, to the north of CLLJ climatological position (Figure 6(b)). Wind speed anomalies are organized in a similar pattern for regime 5 with negative anomalies maximum at 12°N and 82°W and positive anomalies centred at 22°N and 78°W (Figure 5(c)).

For regime 4, the trades are enhanced north of 15°N but weakened between the South American coast and 15°N (Figures 6(b) and (e)). Their weakening acts to reduce moisture divergence over the southeast part of the basin where positive anomalies of specific humidity are found (Figure 5(b), contours), thus leading to enhanced convection and rainfall over the eastern Caribbean and northern South America (Figure 4(d)). Regime 5 is characterized by similar anomalies but shifted westwards following the northwestward propagation of the cyclonic circulation anomaly. Weakened trades south of 15°N (Figures 6(c) and (e)) are also associated with a reduction of moisture divergence, generally associated with strong trades, but this time over central regions of the basin where moisture availability is sustained (Figure 5(d)), in turn increasing convection and rainfall over the central Caribbean (Figure 4(k)). During regime 6, the cyclonic cell is located further west at about 20°N and 85°W and weaker in strength as shown by geopotential anomalies also displaying an anticyclonic feature developing eastwards (Figure 5(e)). Positive wind speed anomalies are maximum just south of Cuba at about 18°N and 82°W, intensifying the CLLJ along its southern branch. This increases moisture availability (Figure 5(f)) and rainfall to the northwest of the Caribbean basin, while drier conditions prevail to the east (Figures 4(f) and (m)). Overall, moisture availability is one of the critical factors determining the strength of convection in the IAS, and the significant contribution from

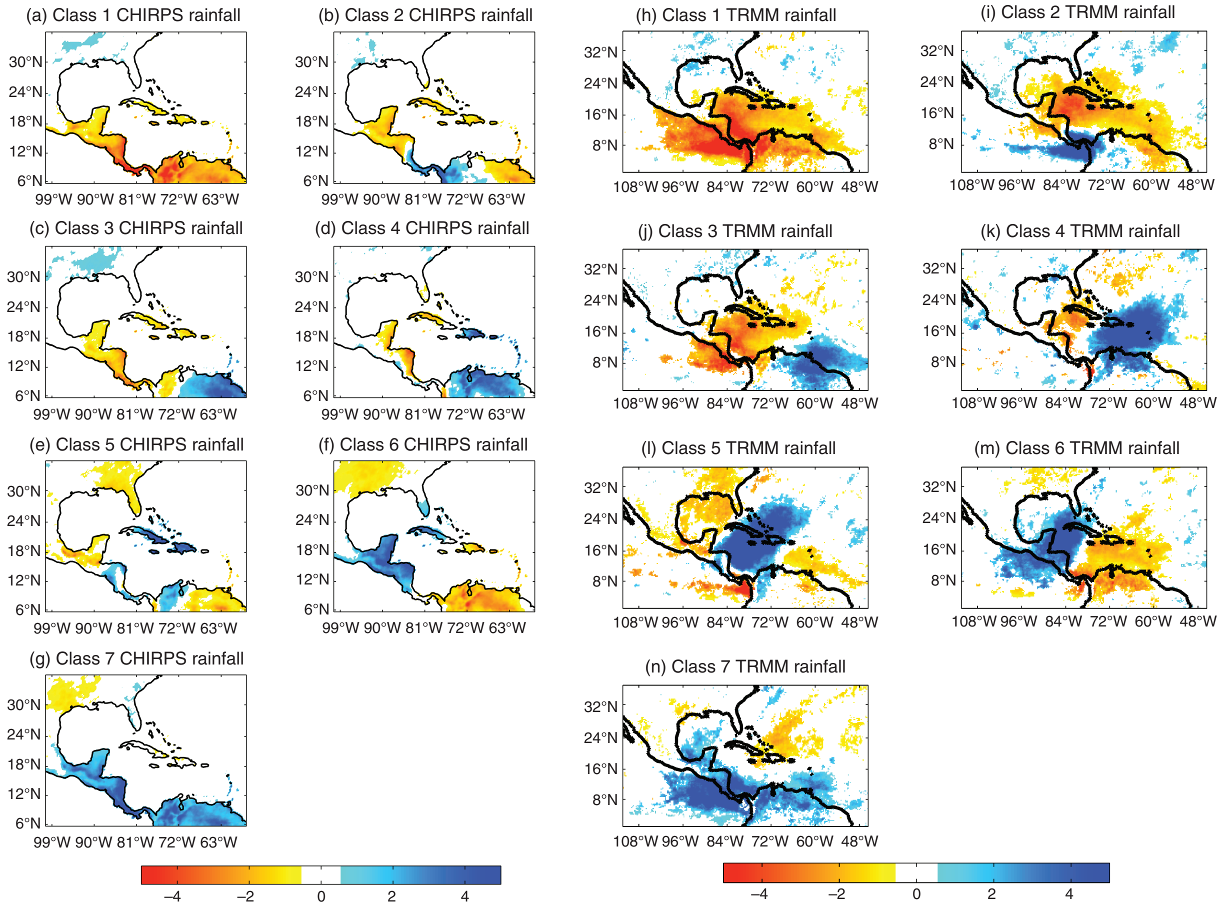

Figure 4. Anomaly composites of 1980–2009 CHIRPS (a–g) and 1998–2009 TRMM (h–n) daily rainfall anomalies for the seven daily OLR regimes occurrences. Only the grid-points for which anomalies are significant at 95% confidence level of Student's *t*-test are displayed (in mm day^{-1}).

the CLLJ during wet regimes 4, 5 and 6 is consistent with earlier studies which identified the Caribbean Sea as the primary source of moisture and the CLLJ as the principal transport mechanism (Duran-Quesada *et al.*, 2010).

Low pressure and cyclonic circulation anomalies similar to those discussed above are also typical of wet regime 7, where they are maximum over Central America (at about 16°N and 90°W), increasing moisture advection from the eastern Pacific through strong westerly anomalies, consistent with Duran-Quesada *et al.* (2010) (not shown). By contrast, dry regimes 1–2 and regime 3 (associated with wettening over the eastern Caribbean and northeastern South America) are all characterized by an anticyclonic circulation anomaly (not shown) that resembles the transient Gulf of Mexico anticyclone highlighted in Chadee and Clarke (2015). This feature acts to strengthen the CLLJ within its southern branch stretching along South America (Figure 6(e)), depriving most of the Caribbean of its moisture inflow, thus reducing convection and rainfall locally (Figures 4(a), (b), (h) and (i)).

4.2. Midlatitude teleconnections

Figure 7 shows anomaly composites for regimes 4–6 plotted over a broad North Atlantic–North America domain. A strong anomalous upper-level ridge is present over eastern North America in regimes 4 and 5, with a deep trough downstream of it that extends into the IAS. The southward incursion of upper-tropospheric negative geopotential anomalies is seen to be associated with the low-pressure convective cell transiting westward in the Tropics with anomalous cyclonic/anticyclonic cells to the northwest/east respectively. Anomalous mid-tropospheric ascent is located to the southeast of the anomalous cyclonic cell center over the Caribbean. The midlatitude wave teleconnection is stronger in regime 4 compared to regime 5, while the anomalous ridge is seen to retrograde southwestwards leading to significant positive pressure anomalies in the upper-troposphere over the southwest United States and negative anomalies over the southeast for regime 6. This sequence of upper-tropospheric configurations is reminescent of the behaviour of potential vorticity (PV) 'streamers' during anticyclonic wave breaking (Thorncroft *et al.*, 1993; Davis, 2010) and which have been related to subtropical cyclone formation in the North Atlantic in previous works (Bentley, 2014). PV streamers inject regions of relatively high upper-tropospheric PV into the subtropical lower troposphere, which become advected westward by the mean easterlies and CLLJ during the sequence of regimes 4–6.

The vertical structure of these convective cells is shown in Figure 8. Low pressure anomalies extend throughout the troposphere in the subtropics (Figures 8(a)–(c)) and

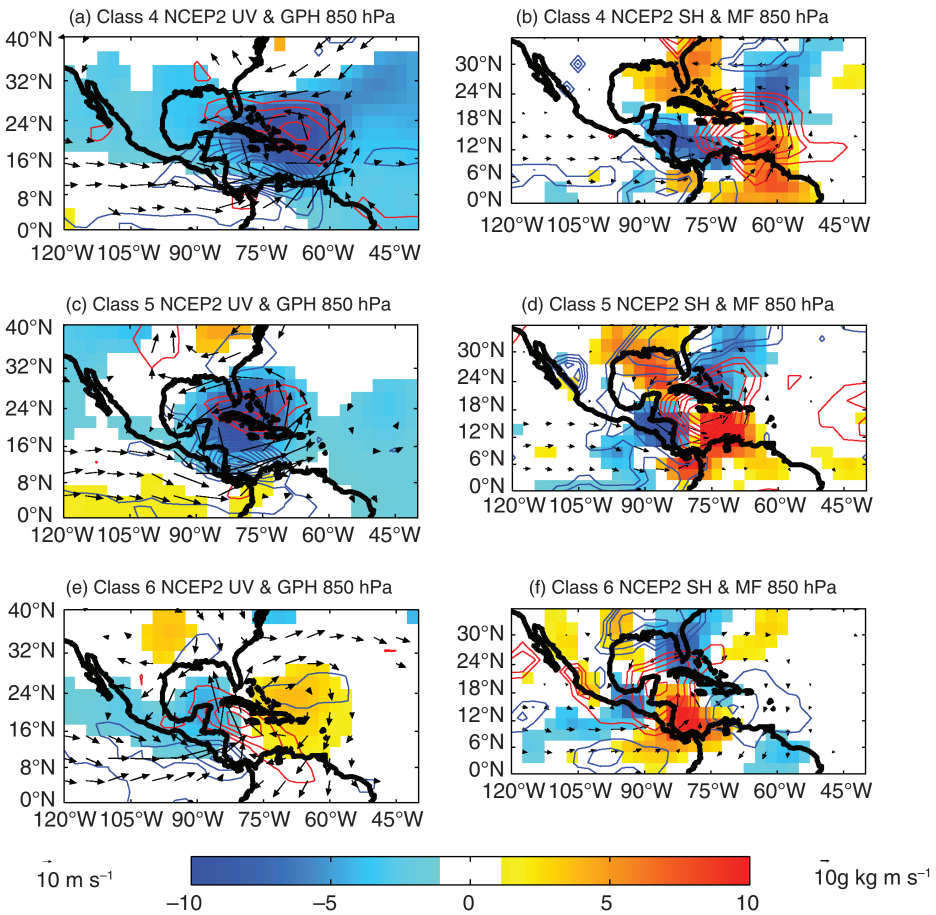

Figure 5. Composites of reanalysis anomaly fields for regimes 4–6. (a), (c) and (e): 850hPa geopotentials (shadings in $m^2 s^{-2}$), winds (vectors in $m s^{-1}$) and wind speed (red/blue contours starting at and every ± 0.25 $m s^{-1}$) anomalies for regimes 4 (a), 5 (c) and 6 (e). (b), (d) and (f): Similar plots but for 850 hPa daily specific humidity (red/blue contours correspond to positive/negatives anomalies starting at and every ± 0.1 $g kg^{-1}$), moisture fluxes (vectors in $g kg^{-1}$ $m s^{-1}$) and convergence (red/blue shadings indicating anomalous convergence/divergence in $g kg^{-1}$ s^{-1}) anomalies (b, d and f). The respective scaling of wind vectors and moisture fluxes is indicated by the arrow key at the bottom left and right respectively, while geopotential and moisture convergence shadings are scaled on the same color bar. Only the grid-points for which anomalies are significant at 95% confidence level of Student's *t*-test are displayed.

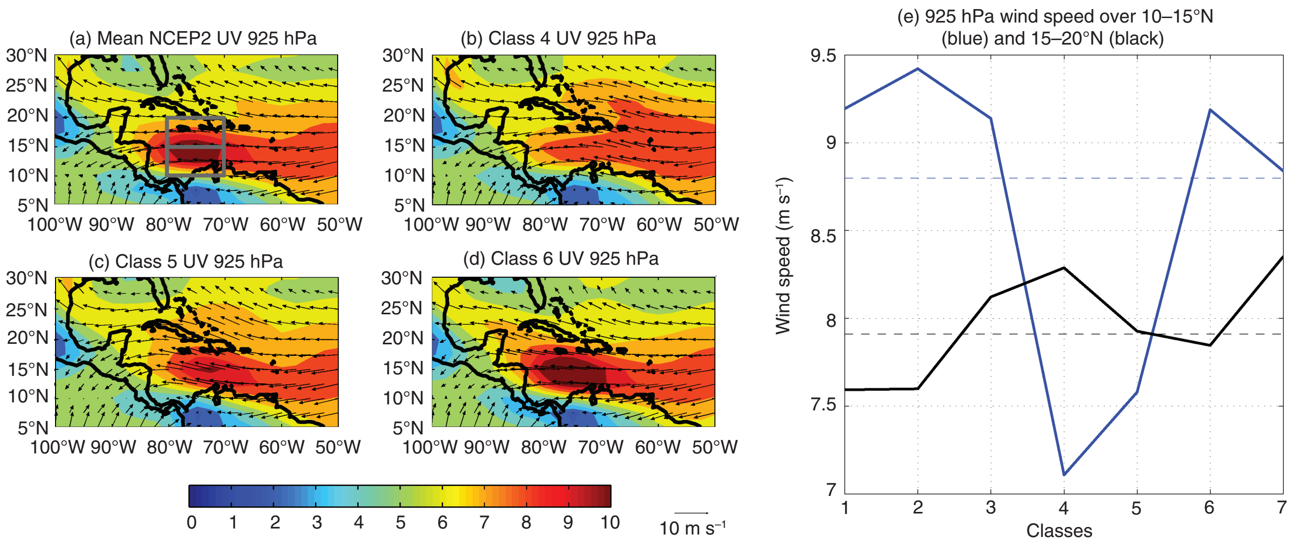

Figure 6. Regime composites of total reanalysis wind fields. (a)–(d): 925 hPa winds (vectors, in $m s^{-1}$) and wind speeds (shadings, in $m s^{-1}$) (a), for regimes 4 (b), 5 (c) and 6 (d). (e): Index of total wind speeds averaged north and south of the CLLJ mean location [(10°–15°N; 70°–80°W) and (15°–20°N; 70°–80°W), see grey boxes in panel a] for the seven daily OLR regimes occurrences (d) together with their 1980–2009 means (dashed lines).

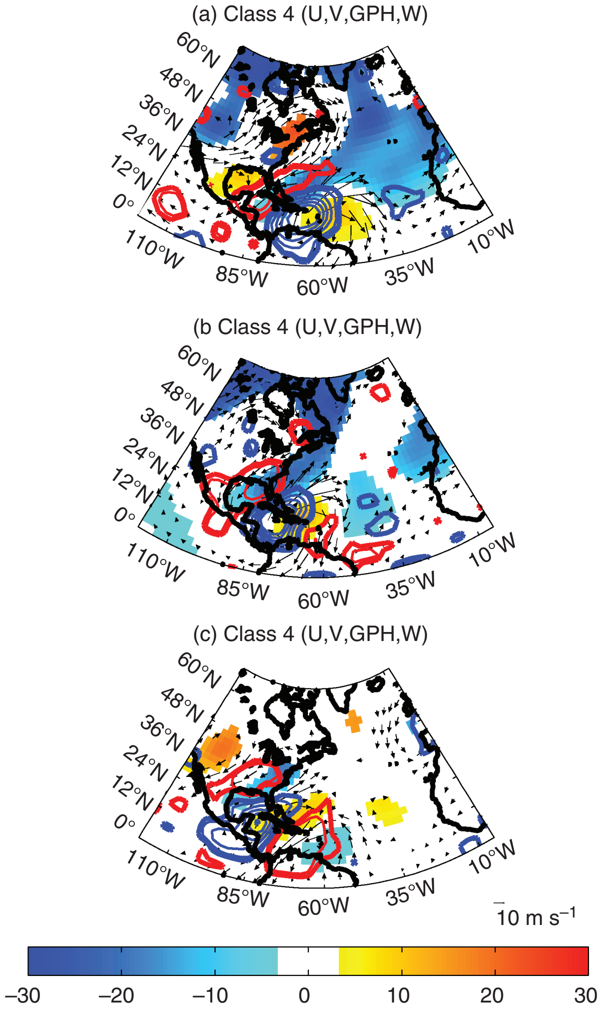

Figure 7. Regimes 4–6 anomaly composites of 200 hPa geopotential (shadings in $m^2 s^{-2}$) and wind (vectors in $m s^{-1}$) with 500 hPa omega vertical velocity (red/blue thick contours at $\pm 5 \times 10^{-3}$ Pa s^{-1} and then every 10^{-2} Pa s^{-1} corresponding to descent/ascent anomalies respectively) anomalies associated to regimes 4 (a), 5 (b) and 6 (c). Only the grid-points for which anomalies are significant at 95% confidence level of Student's *t*-test are displayed (for winds at least one component).

even in the Tropics (Figures 8(d)–(f)), where they transit westwards from about 65° to 90°W from regimes 4 and 5 (consistent with Figures 5(a) and (c)), with maximum anomalous ascent to the east, particularly pronounced above 700 hPa. The latter is part of an anomalous anticlockwise cell in the zonal plane across the convective cell with descent anomalies to the west and anomalous easterly (westerly) flows aloft (at the surface), especially east of 80°W. The low pressure anomalies, increasing with height and extending across the whole troposphere almost vertically in the subtropics (Figures 8(a)–(c)), exhibit the cold core structure of midlatitude troughs characterized by coldest temperatures and lowest pressures at their center where intensity also increases with height (Gill, 1982). In the Tropics, the maximum low-pressure anomalies are seen in the mid-troposphere, decreasing with height (Figures 8(d) and (e)). This structure is more typical of the warm core structure (Gill, 1982) of AEW troughs (Stern and Zhang, 2013), although it may simply reflect down-isentrope PV advection into the Tropics. Maximum ascent anomalies in the Tropics (Figures 8(d)–(f)) are also found east of the anomalous surface low pressure cell center, while maximum descent anomalies are found to the west/northwest, as shown in Figures 7(a)–(c).

4.3. Linkages with tropical easterly waves

Composites of the total zonal wind for each regime are plotted as contours in Figure 8 and indicate marked vertical shear. In the Tropics (lower panels), there are easterlies in the lower troposphere and westerlies aloft, related to the extension of the tropical easterlies and subtropical westerly jet respectively. The low level anomalous easterly flow at 0°–20°N is most pronounced below and to the east of the anomalous low pressure cell for regimes 4 and 5 (Figures 8(d) and (e)), but extends further west for regime 6 (Figure 8(f)) indicating that the wave acts to decrease the westerly vertical shear, typical of a baroclinic wave or of the shear-forced vertical circulations reported by Zhang and Kieu (2005) for TCs evolving in a sheared environment.

Statistically significant mid-tropospheric ascent anomalies can be identified up to 5 days in advance of regime 4 over the western tropical Atlantic near 60°W (Figure 9). These broad scale westward-propagating anomalies bear resemblance to 'suprasynoptic' scale patterns (Persson, 1984) modulating convection over West Africa during the June–September period (Sultan and Janicot, 2003) and which were found to share characteristics of synoptic weather systems associated to AEWs but at larger spatial scale with a similar periodicity and half the propagation speed. AEWs are also known to propagate out in the tropical Atlantic where they can trigger TC formation and given the resemblances to TC dynamics discussed in the previous section, the sequence of regimes 4–6 could be interpreted as a modulation of synoptic-scale easterly waves activity at larger scale. The mid-tropospheric tropical ascent anomalies are seen to merge with the developing anomalous upper-tropospheric anticyclonic wave-breaking pattern emerging from the midlatitudes. Further work is needed to determine the independence of these two precursor phenomena emerging in our regime composites.

4.4. Convective regimes frequency and MJO phases

The frequency of occurrences of the seven regimes is broken down by MJO phases in Figure 10(a). The frequency of wet regimes 4, 5 and 6 is highest during MJO phases 1 and 2, when MJO convection is enhanced over Africa and the western Indian Ocean. This is consistent with Ventrice *et al.* (2011) and Martin and Schumacher (2011) who identified a similar relationship between MJO phases 1–2 *versus* OLR and rainfall respectively over the Caribbean. Figures 10(b)–(d) show the lagged relationship between MJO phase and regimes 4–6 frequency. The MJO's impact on regimes 4–6 frequency during phases 1 and 2 is seen to persist for up to 2 weeks after MJO phase 1 and a week after phase 2, and vanishes once the MJO reaches phase 3 (about 2 weeks after phase 1), with

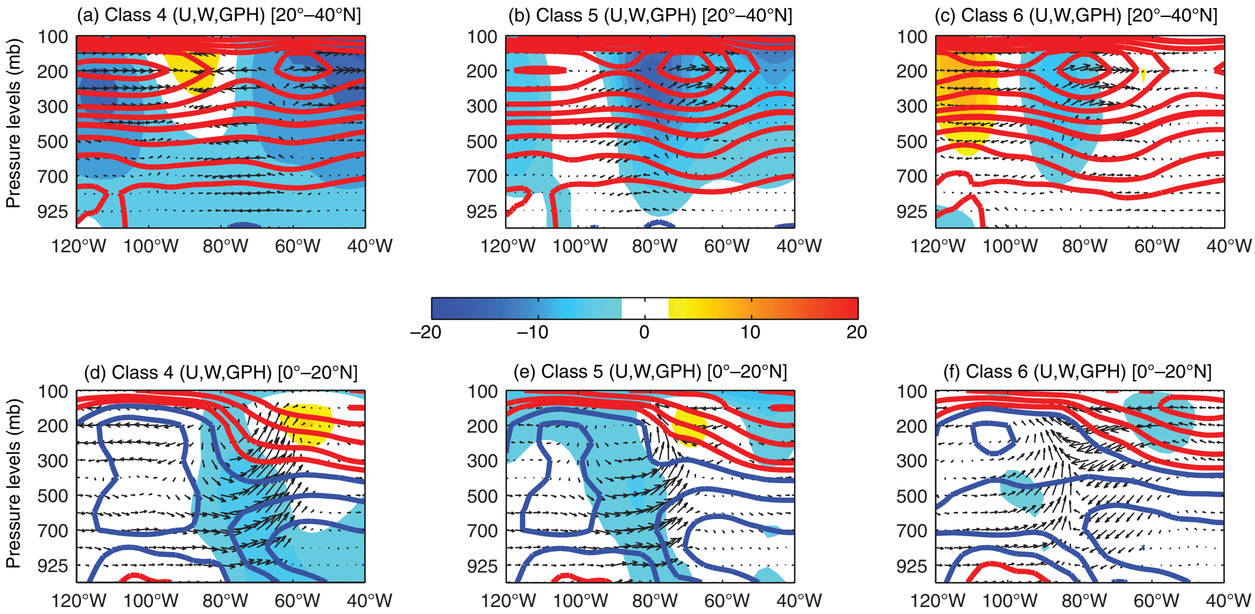

Figure 8. Longitude-pressure cross-sections for regimes 4–6, for the subtropics (a–c) and Tropics (d–f). Geopotential (shadings, $m^2\,s^{-2}$), zonal wind and omega vertical velocity anomalies (vectors scaled at 1 unit/degree with vertical velocity magnified) averaged between (0°–20°N) (bottom) and (20°–40°N) (top) for daily OLR regimes 4, 5 and 6 occurrences. Thick red/blue contours correspond to the mean westerly/easterly flows prevailing during each regime (starting at ±1 and every $2\,m\,s^{-1}$). Only the grid-points for which anomalies are significant at 95% confidence level of Student's *t*-test are displayed (for vectors at least one component).

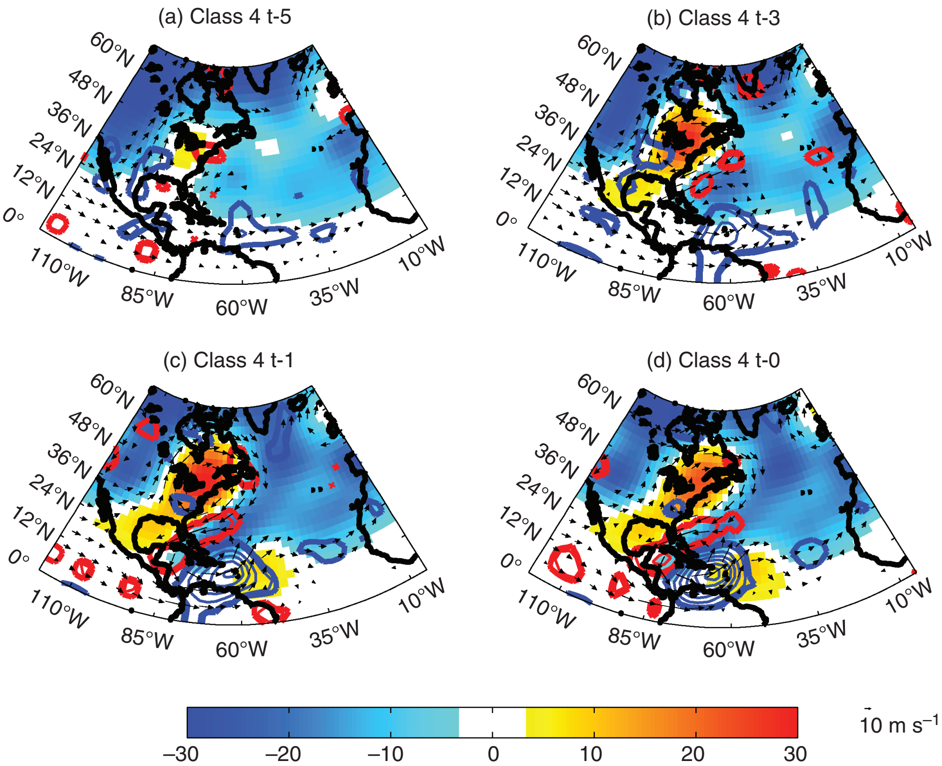

Figure 9. Composites of NCEP2 600 hPa winds (vectors) and omega vertical velocity (red/blue contours thick at $\pm 5 \times 10^{-3}\,Pa\,s^{-1}$ and every $10^{-2}\,Pa\,s^{-1}$ corresponding to descent/ascent anomalies respectively) and 200 hPa geopotential (shadings in $m^2\,s^{-2}$) anomalies at 5, 3, 1 days lead (a–c) and no lead (d) for NOAA daily OLR regime 4.

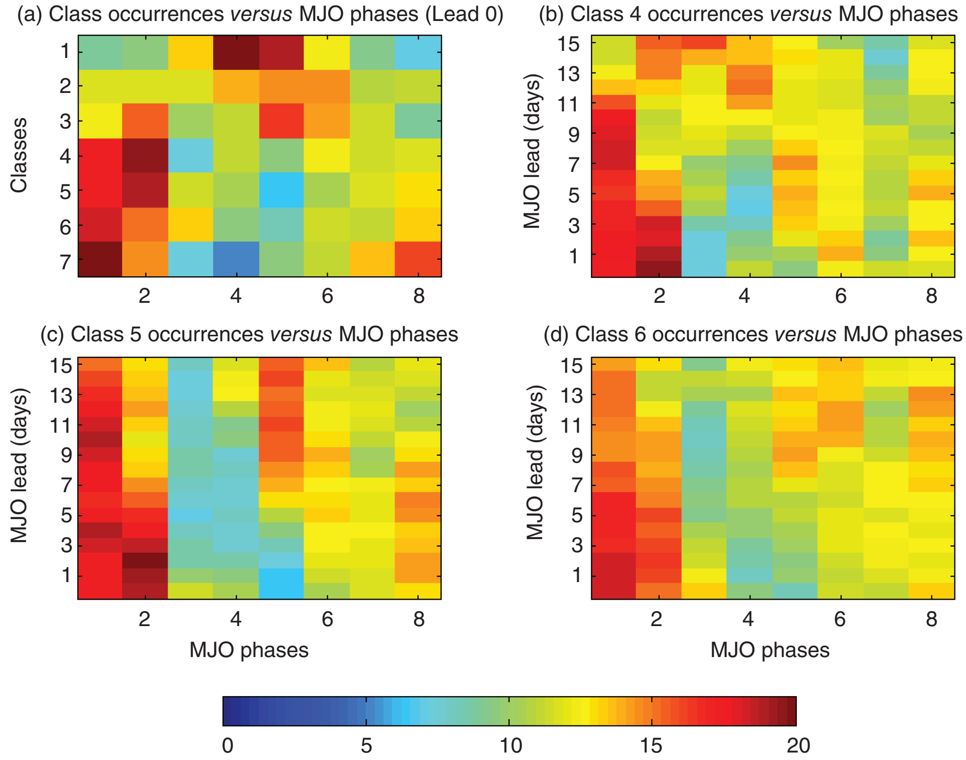

Figure 10. Fraction of regimes 4 (b), 5 (c) and 6 (d) occurrences relative to the total number of days spent in each class (colours, in percent) for each phase of the MJO over the 1980–2009 period. The ordinate in panels b–d shows the number of days that the MJO phase precedes the daily OLR classes from 0 to 15 days, while the contingency matrix at zero lead is plotted in panel a.

MJO convection located over the eastern Indian Ocean. This MJO impact on the Caribbean is argued by Ventrice *et al.* (2011) to be via equatorial Rossby waves emanating from the MJO-enhanced convection over Africa and that interact with AEWs. The MJO's impact on regimes 4–6 frequency shown in Figure 10 thus provides additional evidence for the role played by easterly waves in generating the westward-propagating convection anomalies represented by these regimes.

5. Summary and conclusions

This study has analysed sub-seasonal convection variability using a clustering approach (*k*-means) applied to anomalies (defined with respect to the mean seasonal cycle) of 2.5° gridded daily NOAA OLR observations for a 30-year-period (1980–2009) to identify recurrent weather types for the May–November period, and their related atmospheric circulation anomalies. A particular focus is given to potential interactions between the Tropics and midlatitudes, as well as their relationships to IAS rainfall and large-scale SSTs in the neighbouring oceanic basins. Seven patterns of anomalous convection are identified, each related to distinct rainfall anomalies over parts of the region. A very close relationship is found between regime anomaly fields of OLR and two different gridded rainfall datasets. Three regimes of suppressed convection (regimes 1, 2 and 3) represent almost half of the days of the May to November season, regime 1 being the most persistent (Table 1). They are most predominant during the MSD, counterbalancing the reduced frequency of the regimes of anomalously enhanced convection in those calendar months (Figure 3). Regimes 1, 2 and 3 are all associated with anomalous anticyclonic circulation anomalies over the Gulf of Mexico acting to strengthen the southern branch of the CLLJ (10°–15°N, Figure 6(e)), depriving most of the Caribbean of moisture inflow. The remaining regimes are all related to enhanced convection and cyclonic circulation anomalies over the Caribbean. For one wet regime (regime 7) most frequent in July, the cyclonic anomaly is located over Central America and acts to increase moisture advection from the eastern Pacific through strong westerly wind anomalies, and thus rainfall over Central and South America to the disadvantage of northern regions of the Caribbean (Figures 4(g) and (n)).

Wet regimes 4 and 5, most frequent from August onwards, as well as regime 6, which shows less seasonality, are characterized by anomalous cyclonic cells propagating northwestwards across the Caribbean basin. These lead to a weakening (strengthening) of the CLLJ along its southern (northern) branches, exposing most of the Caribbean to increased trade-wind moisture inflow (Figure 6). These regimes resemble the weather types 4 and 5 recently identified by Moron *et al.* (2015) from a cluster analysis of *total* daily OLR and wind fields – in contrast to our analysis of OLR anomalies defined with respect to the mean seasonal cycle of OLR. The sequence of anomaly composites for regimes 4, 5 and 6 exhibits relationships to the southward incursion of synoptic-scale

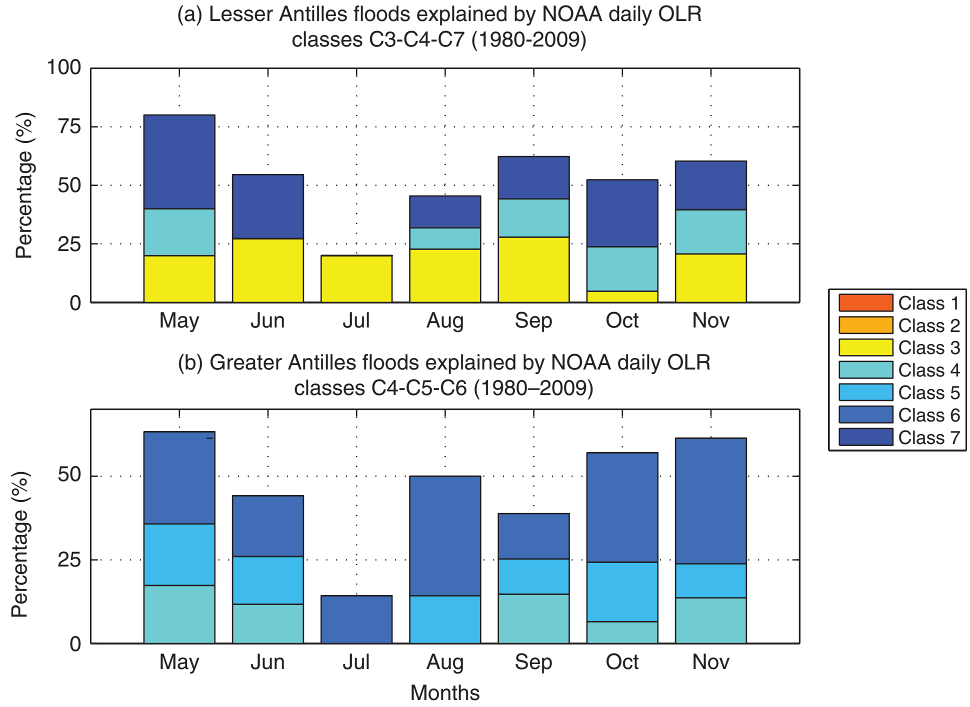

Figure 11. Percentage of floods reported in the Caribbean Disaster Impacts and Preparedness database each month from May to November over the last 30 years in the Lesser/Greater Antilles explained by wet regimes (a and b).

Rossby waves from the midlatitudes (Figures 7–9). More work is required to fully understand this mechanism, but our results suggest that the anticyclonic wave breaking documented by Thorncroft *et al.* (1993) is occurring. The advection of high PV from midlatitude stratosphere southward and down the isentropes could thus contribute to the westward propagation of the regimes 4–6 progression.

However, the broad scale westward-propagating convection anomalies associated with these regimes can also be interpreted, in the context of 'suprasynoptic' scales (Persson, 1984), as sub-seasonal modulations of easterly waves synoptic-scale activity as evidenced by Sultan and Janicot (2003) over West Africa in connection with AEWs that are also known to propagate out in the tropical Atlantic where they can trigger TC development. Evidence of easterly wave precursors is perhaps most obviously seen in the relationship between regime frequency and the MJO. The enhanced (suppressed) convection regimes tend to be more frequent during MJO phases 1 and 2 (4–6) (Figure 10). This is consistent with MJO relationships to Caribbean convection (Ventrice *et al.*, 2011), and with rainfall and modulations of the CLLJ (Martin and Schumacher, 2011). Ventrice *et al.* (2011) demonstrate that MJO convection anomalies over Africa during phases 1 and 2 emit equatorial Rossby waves that lead to enhanced convection over the Caribbean and more Atlantic tropical cyclogenesis.

It is worth noting that out of five major hurricanes corresponding to the sequence of regimes 4, 5 and 6, four were also related to AEW (Opal, Ivan, Dennis and Ike) and four to upper-level midlatitude troughs (Opal, Ivan, Wilma and Ike). Thus, Opal, Ivan and Ike were associated with both remote impacts occurring simultaneously. More work is needed to determine their respective roles, although large amplitude is to be expected when both occur simultaneously and interfere constructively. Moreover, wet regimes occurrences are found to be concurrent with island-scale flood episodes archived in the Caribbean Disaster Impacts and Preparedness database at the Caribbean Institute for Meteorology and Hydrology (CIMH). As shown in Figure 11, >50% of the floods recorded over the Lesser/Greater Antilles almost every months (except July)/in May, October and November of the 1980–2009 period respectively correspond to occurrences of wet regimes 3–4–7/4–5–6 suggesting their relevance to flood predictability.

The results presented here are based on coarse spatial resolution OLR data suggesting that a similar set of regimes could be identified and used as a diagnostic of General Circulation Model (GCM) forecast products. The evidence that some of the most devastating hurricanes and flood episodes in the Caribbean in the last 30 years developed within such atmospheric conditions is a direct motivation for further studies, in particular through dynamical experiments that will help to examine deeper the mechanisms at play and will thus benefit ongoing prediction efforts in the IAS region.

Acknowledgements

We wish to thank Kelli Armstrong for providing analyses on the Caribbean Disaster Impacts and Preparedness database, and three reviewers whose insightful comments resulted in substantial improvements to the manuscript. N. Vigaud was supported by funding from NOAA's International Research and Application Project (IRAP) NA13OAR4310184 grant and an NOAA Sectoral Applications Research Program (SARP) NA14OAR4310256 grant. A. W. Robertson was supported by grant ONR-MURI N00014-12-1-0911 from the Office of Naval Research. The IRI Data Library (http://iridl.ldeo.clumbia.edu) was used to access NOAA OLR and OISST, NOAA Unified and CHIRPS rainfall datasets, TRMM estimates and NCEP2 re-analyses.

References

Aiyyer A, Thorncroft C. 1997. Climatology of vertical wind shear over the tropical Atlantic. *J. Clim.* **19**: 2969–2982.

Amador J. 1998. The trade wind easterly jet. *Top. Meteorol. Oceanogr.* **5**: 91–102.

Amador J. 2008. Trends and directions in climate research. *Ann. N.Y. Acad. Sci.* **1146**: 153–188.

Angeles ME, Gonzalez JE, Ramirez-Beltran ND, Tepley CA, Comarazamy DE. 2010. Origin of the Caribbean rainfall bimodal behaviour. *J. Geophys. Res.* **115**: D11106, doi: 10.1029/2009JD012990.

Bentley A. 2014. *Upper-Tropospheric Precursors Associated with Subtropical Cyclone Formation in the North Atlantic Basin*. Master's thesis, State University of New York.

Carlson T. 1969. Some remarks on African disturbances and their progress over the tropical Atlantic. *Mon. Weather Rev.* **97**: 716–726.

Chadee X, Clarke R. 2015. Daily near-surface large-scale atmospheric circulation patterns over the wider Caribbean. *Clim. Dyn.* **44**: 2927–2946.

Chang P, Saravanan R, Ji L. 2003. Tropical Atlantic seasonal predictability: the roles of El Niño remote influence and thermodynamic air-sea feedback. *Geophys. Res. Lett.* **20**(10): 1501, doi: 10.1029/2002GL016119.

Chen A, Taylor M. 2002. Investigating the link between early season Caribbean rainfall and El Niño +1. *Int. J. Climatol.* **22**: 87–106.

Cheng X, Wallace J. 2003. Regime analysis of the Northern Hemisphere winter-time 500 hPa height field: spatial patterns. *J. Atmos. Sci.* **50**: 2674–2696.

Cook K, Vizy E. 2010. Hydrodynamics of the Caribbean Low Level Jet and its relationship to precipitation. *J. Clim.* **23**: 1477–1494.

Davis C. 2010. Simulations of subtropical cyclones in a baroclinic channel model. *J. Atmos. Sci.* **138**: 2953–2974, doi: 10.1175/2010JAS3411.1.

Duran-Quesada AM, Gimeno L, Amador JA, Nieto R. 2010. Moisture sources for Central America: identification of moisture sources using a Lagrangian analysis technique. *J. Geophys. Res.* **115**: D05103, doi: 10.1029/2009JD012455.

Enfield D, Alfaro E. 1999. The dependence of the Caribbean rainfall on the interaction of the tropical Atlantic and Pacific Oceans. *Geophys. Res. Lett.* **23**: 3305–3308.

Enfield DB, Mayer DA. 1997. Tropical Atlantic SST variability and its relation to El Niño-Southern Oscillation. *J. Geophys. Res.* **102**: 929–945.

Fauchereau N, Pohl B, Reason C, Rouault M, Richard Y. 2009. Recurrent daily OLR patterns in the Southern Africa/Southwest Indian Ocean region, implications for South African rainfall and teleconnections. *Clim. Dyn.* **32**: 575–591.

Figueroa S, Nobre C. 1990. Precipitation distribution over central and western tropical South America. *Climanalise* **5**: 36–44.

Frank W, Roundy PE. 2006. The role of tropical waves in tropical cyclogenesis. *Int. J. Climatol.* **28**: 2397–2417.

Funk C, Peterson P, Landsfeld M, Pedreros D, Verdin J, Rowland J, Romero B, Husak G, Michaelsen J, Verdin A. 2014. A quasi-global precipitation time-series for drought monitoring. *US Geological Survey Data Series*, 832, 4p.

Funk C, Peterson P, Landsfeld M, Pedreros D, Verdin J, Shukla S, Husak G, Rowland J, Harrison L, Hoell A, Michaelsen J. 2015. The climate hazards infrared precipitation with stations – a new environmental record for monitoring extremes. *Sci. Data* **2**: 1–21, doi: 10.1038/sdata.2015.66.

Ghil M, Robertson AW. 2002. "Waves" vs. "particles" in the atmosphere's phase space: a pathway to long-range forecasting? *Proc. Natl. Acad. Sci. U. S. A.* **99** (Suppl. 1): 2493–2500.

Giannini A, Kushnir Y, Cane M. 2000. Interannual variability of Caribbean rainfall, ENSO, and the Atlantic Ocean. *J. Clim.* **13**: 297–311.

Giannini A, Kushnir Y, Cane M. 2001. Interdecadal changes in the ENSO teleconnections to the Caribbean region and the North Atlantic Oscillation. *J. Clim.* **14**: 2867–2879.

Gill AE. 1982. Atmosphere–ocean dynamics. International Geophysical Series, vol. 30, 662 pp.

Hastenrath S. 1984. Interannual variability and annual cycle: mechanisms of circulation and climate in the tropical Atlantic sector. *Mon. Weather Rev.* **112**: 1097–1107.

Hastenrath S, Lamb P. 1977. Some aspects of circulation and climate over the eastern equatorial Atlantic. *Mon. Weather Rev.* **105**: 1019–1023.

Hidalgo H, Duran-Quesada A, Amador J, Alfaro E. 2015. The Caribbean low-level jet, the Inter-Tropical Convergence Zone and precipitation patterns in the Intra-Americas Sea: a proposed dynamical mechanism. *Geogr. Ann. Ser. B* **97**: 41–59.

Higgins R, Rao Y, Wang X. 1997. Influence of the North American monsoon system on the United States summer precipitation regime. *J. Clim.* **10**: 2600–2622.

Huffman G, Adler R, Bolvin D, Nelkin E. 2010. *The TRMM Multi-satellite Precipitation Analysis TMPA. Chapter 1 in Satellite Rainfall Application for Surface Hydrology*, ISBN 978-90-481-2914-0. Springer Verlag, 3–22.

Kanamitsu M, Ebisuzaki W, Woollen J, Yang S-K, Hnilo J, Fiorino M, Potter GL. 2002. NCEP-DOE AMIP-2 Reanalysis (R-2). *Bull. Atmos. Meteorol. Soc.* **83**: 1631–1643.

Kerns B, Greene K, Zipser E. 2008. Four years of tropical ERA-40 vorticity maxima tracks. Part I: climatology and vertical vorticity structure. *Mon. Weather Rev.* **136**: 4301–4319.

Kossin J, Camargo S, Sitkowski M. 2010. Climate modulation of the North Atlantic hurricane tracks. *J. Clim.* **23**: 3057–3076.

Leroux L, Hall S. 2010. On the relationship between African easterly waves and the African easterly jet. *J. Atmos. Sci.* **66**: 2303–2316.

Liebmann B, Smith C. 1996. Description of a complete (interpolated) outgoing longwave radiation dataset. *Bull. Am. Meteorol. Soc.* **83**: 1631–1643.

Magana V, Amador J, Medina S. 1999. The midsummer drought over Mexico and America. *J. Clim.* **12**: 1577–1588.

Martin E, Schumacher C. 2011. Modulation of Caribbean precipitation by the Madden-Julian Oscillation. *J. Clim.* **24**: 813–824, doi: 10.1175/2010JCLI3773.1.

Michelangeli P, Vautard R, Legras B. 1995. Weather regime occurrence and quasi-stationarity. *J. Atmos. Sci.* **52**: 1237–1256.

Mock C. 1996. Climate controls and spatial variations of precipitation in the western United States. *J. Clim.* **9**: 1111–1125.

Molinari J, Knight D, Dickinson M, Vollaro D, Skubis S. 1996. Potential vorticity, easterly waves, and eastern Pacific tropical cyclogenesis. *Mon. Weather Rev.* **125**: 2699–2708.

Moron V, Plaut G. 2003. The impact of El Niño-Southern Oscillation upon weather regimes over Europe and the North Atlantic during boreal winter. *Int. J. Climatol.* **23**: 363–379.

Moron V, Robertson A, Ward M, Ndiaye O. 2008. Weather types and rainfall over Senegal. Part I: observational analysis. *J. Clim.* **21**: 266–287.

Moron V, Gouirand I, Taylor M. 2015. Weather types across the Caribbean basin and their relationship with rainfall and sea-surface temperatures. *Clim. Dyn.* **47**: 601–621, doi: 10.1007/s00382-015-2858-9.

Persson A. 1984. The use of spectrally filtered products in medium-range forecasting. *ECMWF Tech. Memo.* **90**, 1–47.

Reynolds RW, Smith TM, Liu C, Chelton D, Casey K, Schlax M. 2007. Daily high-resolution-blended analyses for sea surface temperature. *J. Clim.* **20**: 5473–5496.

Riehl H. 1945. Waves in the easterlies and the polar front in the tropics. *Miscellaneous Report*, Department of Meteorology, University of Chicago.

Riehl H. 1948. On the formation of west Atlantic hurricanes. *Miscellaneous Report*, Department of Meteorology, University of Chicago.

Ropolewski C, Halpert M. 1987. Global and regional scale precipitation patterns associated with the El-Niño-Southern Oscillation. *Mon. Weather Rev.* **115**: 1606–1626.

Saenz F, Duran-Quesada A. 2015. A climatology of low level wind regimes over Central America using a weather type classification approach. *Front. Earth Sci.* **3**(15): 1–15, doi: 10.3389/feart.2015.00015.

Serra Y, Kiladis G, Hodges K. 2010. Tracking and mean structure of easterly waves over the Intra-Americas Sea. *J. Clim.* **23**: 4823–4840.

Serra Y, Braun J, Adams D. 2016. Observing the Intra-Americas Sea climate: existing and emerging technologies. *US Cliv. Var.* **14**: 1–9.

Shapiro L. 1996. The three-dimensional structure of synoptic-scale disturbances over the tropical Atlantic. *Mon. Weather Rev.* **114**: 1876–1891.

Stern D, Zhang F. 2013. How does the eye warm? Part I: a potential temperature budget analysis of an idealized tropical cyclone. *J. Atmos. Sci.* **70**: 73–90, doi: 10.1175/JAS-D-11-0329.1.

Sultan B, Janicot S. 2003. The West African monsoon dynamics. Part I: documentation of intraseasonal variability. *J. Clim.* **16**(21): 3389–3406.

Taylor MA, Enfield DB, Chen AA. 2002. Influence of the tropical Atlantic versus the tropical Pacific on Caribbean rainfall. *J. Geophys. Res.* **107**: 3127, doi: 10.1029/2001JC001097.

Taylor MA, Stephenson TS, Owino A, Chen AA, Campbell JD. 2011. Tropical gradient influences on Caribbean rainfall. *J. Geophys. Res.* **116**: D00Q08, doi: 10.1029/2010JD015580.

Thorncroft C, Hodges K. 2001. African Easterly Waves variability and its relationship to Atlantic tropical cyclone activity. *J. Clim.* **14**: 1166–1179.

Thorncroft C, Hoskins B, McIntyre M. 1993. Two paradigms of baroclinic-wave life-cycle behaviour. *Q. J. R. Meteorol. Soc.* **119**: 17–55, doi: 10.1002/qj.49711950903.

Thorncroft C, Parker D, Burton R, Diop M, Ayers J, Barjat H, Deveneau S, Diongue A, Dumelow R, Kindred D, Price N, Saloum M, Taylor C, Tompkins A. 2003. The JET2000 project: aircraft observations of the African easterly jet and African easterly waves. *Bull. Am. Meteorol. Soc.* **84**: 337–351.

Vautard R, Mo K, Ghil M. 1990. Statistical significance test for transition matrices of atmospheric Markov chains. *J. Atmos. Sci.* **47**: 1926–1931.

Ventrice M, Thorncroft C, Roundy P. 2011. The Madden-Julian Oscillation influence on African easterly waves and downstream cyclogenesis. *Mon. Weather Rev.* **139**: 2704–2722.

Vigaud N, Pohl B, Cretat J. 2012. Tropical-temperate interactions over southern Africa simulated by a regional climate model. *Clim. Dyn.* **39**: 2895–2916, doi: 10.1007/s00382-012-1314-3.

Vigaud N, Lyon B, Giannini A. 2017. Sub-seasonal teleconnections between convection over the Indian Ocean, East African long rains and tropical Pacific surface temperatures. *Int. J. Climatol.* **37**: 1167–1180, doi: 10.1002/joc.4765.

Wang C. 2007. Variability of the Caribbean Low-Level Jet and its relation to climate. *Clim. Dyn.* **29**: 411–422.

Wang C, Lee S-K. 2007. Atlantic warm pool, Caribbean Low Level Jet, and their potential impact on Atlantic hurricanes. *Geophys. Res. Lett.* **34**: L02703, doi: 10.1029/2006GL028579.

Wang C, Enfield D, Lee S, Landsea C. 2006. Influences of the Atlantic warm pool on Western Hemisphere summer rainfall and Atlantic hurricanes. *J. Clim.* **19**: 3011–3028.

Wang C, Lee S-K, Mechoso C. 2010. Interhemispheric influence of the Atlantic Warm Pool on the Southeastern Pacific. *J. Clim.* **23**: 404–418.

Whyte F, Taylor M, Campbell J. 2008. Features of the Caribbean low level jet. *Int. J. Climatol.* **28**: 119–128.

Wu R, Kirtman B. 2010. Rainy season Caribbean Sea precipitation and ENSO. *COLA Tech. Rep.* **302**: 1–49.

Xie S-P, Carton J. 2004. *Tropical Atlantic Variability: Patterns, Mechanisms and Impacts*. American Geophysical Union Geophysical Monograph.

Yanai M. 1968. Evolution of a tropical disturbance in the Caribbean Sea region. *J. Meteorol. Soc. Jpn.* **46**(2): 86–108.

Yu W, Han W, Maloney ED, Gochis D, Xie S-P. 2011. Observations of eastward propagation of atmospheric intraseasonal oscillations from the Pacific to the Atlantic. *J. Geophys. Res.* **116**: D02101, doi: 10.1029/2010JD014336.

Zhang D-L, Kieu CQ. 2005. Shear-forced vertical circulations in tropical cyclones. *Geophys. Res. Lett.* **32**: L13822, doi: 10.1029/2005 GL023146.

